Laboratory Investigations of Low-Swirl Injectors Operating With Syngases

David Littlejohn

Robert K. Cheng

Environmental Energy Technology Division,
Lawrence Berkeley National Laboratory,
Berkeley, CA 94720

D. R. Noble

Tim Lieuwen

School of Aerospace Engineering,
Georgia Institute of Technology,
Atlanta, GA 30332

The low-swirl injector (LSI) is a lean premixed combustion technology that has the potential for adaptation to fuel-flexible gas turbines operating on a variety of fuels. The objective of this study is to gain a fundamental understanding of the effect of syngas on the LSI flame behavior, the emissions, and the flowfield characteristics for adaptation to the combustion turbines in integrated gasification combined cycle clean coal power plants. The experiments were conducted in two facilities. Open atmospheric laboratory flames generated by a full size (6.35 cm) LSI were used to investigate the lean blow-off limits, emissions, and the flowfield characteristics. Verification of syngas operation at elevated temperatures and pressures were performed with a reduced scale (2.54 cm) LSI in a small pressurized combustion channel. The results show that the basic LSI design is amenable to burning syngases with up to 60% H_2. Syngases with high H_2 concentration have lower lean blow-off limits. From particle image velocimetry measurements, the flowfield similarity behavior and the turbulent flame speeds of syngases flames are consistent with those observed in hydrocarbon and pure or diluted hydrogen flames. The NO_x emissions from syngas flames show log-linear dependency on the adiabatic flame temperature and are comparable to those reported for the gaseous fuels reported previously. Successful firing of the reduced-scale LSI at 450 $K < T < 505$ K and 8 atm verified the operability of this concept at gas turbine conditions. [DOI: 10.1115/1.3124662]

1 Introduction

The objective of our research is to adapt the low-swirl combustion concept to the gas turbines in integrated gasification combined cycle (IGCC) power plant that burn syngases derived from gasification of coal. Low-swirl combustion is a novel lean premixed combustion method that has been commercialized for industrial heaters. Low-swirl injectors (LSIs) for gas turbines have also been developed for natural gas engines of 5–7 MW in partnership with Solar Turbines of California and for microturbines of 100 kW in partnership with Elliott Energy Systems of Florida [1,2].

To verify the feasibility of the LSI for IGCC combustion turbines, our previous study reported laboratory experiments at atmospheric condition that demonstrated LSI operation with H_2 and diluted H_2 [3]. The velocity data obtained from particle image velocimetry (PIV) showed that the overall flowfield features of the H_2 flames are not significantly different than those of the hydrocarbon flames. The turbulent flame speeds of the H_2 flames correlate linearly with turbulence intensity u'. The value of the turbulent flame speed correlation constant is about 50% higher than the constant determined for the hydrocarbon flames. Comparison of the mean and rms velocity profiles showed that the nearfields of the H_2 flames exhibit self-similarity features that are consistent with those found in hydrocarbon flames. Therefore, the LSI mechanism is not sensitive to the differences in the hydrocarbons and H_2 flame properties and the LSI concept is amenable to burning of H_2.

This paper reports a study of LSI operation with syngases. The syngases derived from gasification of coal generally consist of a blend of H_2 and CO, CO_2, CH_4, and other diluents such as N_2 and steam. The concentration of each constituent varies depending on the type of coal that is being gasified and the heat content of the syngases is generally lower than natural gas. Our previous studies showed that the LSI can deliver <5 ppm NO_x (at 15% O_2) performance while burning fuels of a wide range of heating contents [2–5]. This can be explained by invoking an analytical model that describes the coupling of the self-similar features of the LSI nearfield to the turbulent flame speed S_T. Additionally, these studies showed that lean blow-off limits are insensitive to bulk flow velocity U_0 and the NO_x emissions from atmospheric LSI flames have log-linear dependency on the adiabatic flame temperature T_{ad}. The feasibility of operating the LSI with syngases has already been demonstrated in a study by Sequera and Agrawal [6]. The goal of this paper is to conduct laboratory experiments at atmospheric pressure to determine the lean blow-off limits and obtain more NO_x emissions from syngases to verify the log-linear dependency. Velocity statistics obtained by PIV were used to determine if the analytical model also applies to syngas operation. These were followed by verification of LSI operation at high temperatures and pressures using a reduced scale prototype.

2 Background

The LSI is based on an aerodynamic flame stabilization method that utilizes a divergent flow to sustain a detached propagating premixed turbulent flame [7]. The divergent flow is formed only when the swirl intensities are well below the critical vortex breakdown threshold. Linear decay of the axial velocity within the divergent flow allows the flame to settle where the local velocity is equal and opposite of the turbulent flame speed. Matching the flowfield velocities to the turbulent flame speed is therefore the critical design criterion.

The key component of the LSI is a swirler that supplies the reactants through two passages: an outer annular region with swirl vanes and an open center-channel that allows a portion of the reactants to remain unswirled [8] (Fig. 1). The supply of unswirled reactants through its center is the unique feature of the LSI and its presence retards the formation of a central recirculation zone and promotes the formation of flow divergence. The

Contributed by the International Gas Turbine Institute of ASME for publication in the JOURNAL OF ENGINEERING FOR GAS TURBINES AND POWER. Manuscript received April 4, 2008; final manuscript received May 12, 2008; published online September 30, 2009. Review conducted by Dilip R. Ballal. Paper presented at the ASME Turbo Expo 2008: Land, Sea, and Air (GT2008), Berlin, Germany, June 9–13, 2008.

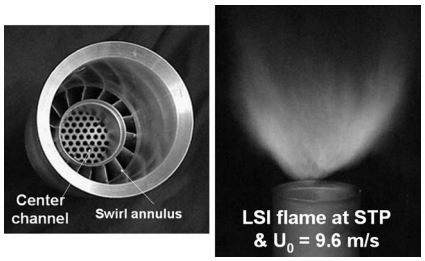

Fig. 1 LSI prototype for Taurus 70 engine

lift-off position of the detached flame is controlled by the divergence rate that can be adjusted by changing the flow split between the swirled and the unswirled flows. The most convenient means to change the flow split is by varying the blockage ratio of the perforated screen covering the center-channel.

The LSI of Fig. 1 utilizes an annular vane swirler for Solar Turbine's T70 SoLoNOx injector [1]. To convert the swirler from high-swirl to low-swirl operation, its center bluff body is removed and replaced by a perforated plate whose blockage ratio is selected to give a swirl number S of 0.4–0.55. The swirl number is defined as [8]

$$S = \frac{2}{3}\tan\alpha\frac{1-R^3}{1-R^2+[m^2(1/R^2-1)^2]R^2} \quad (1)$$

where α is the vane angle and $R=R_c/R_i$. The parameter $m=m_c/m_s$ is the ratio between the mass fluxes of the unswirled m_c and the swirled m_s flows. It is inversely proportional to the blockage ratio of the perforated plate. The SoLoNOx swirler has an internal radius of 3.175 cm and consists of 16 curved vanes with a discharge angle $\alpha=40$ deg. The center-channel to injector radius ratio R is 0.63. As reported in Ref. [2] a fully functional LSI has been developed. Test results showed that the LSI meets all the operational and performance requirements of the T70 engine.

The scientific foundation obtained for the LSI has provided useful insights for its adaptation to gas turbines [9–14]. Analyses of the velocity measurements show that the LSI nearfield exhibits self-similarity behavior. Two parameters deduced from the centerline velocity profiles are invoked to characterize self-similarity [4,5]. They are the virtual origin of the divergent flow x_0, and the nondimensional axial aerodynamic stretch rate a_x. To characterize the flame, the local turbulent flame speeds S_T and the position of the leading edge of the flame brush x_f both determined at the centerline are used. Analysis of S_T shows a linear dependency on turbulence intensity u'. An analytical equation (Eq. (2)) for the velocity balance at x_f shows that a coupling of the self-similar flowfield and a linear turbulent flame speed correlation with u' is the reason why the LSI flame remains stationary through a wide range of velocities and fuel air equivalence ratios ϕ.

$$1-\frac{dU}{dx}\frac{(x_f-x_o)}{U_0}=\frac{S_T}{U_0}=\frac{S_L}{U_0}+\frac{Ku'}{U_0} \quad (2)$$

The two terms on the far RHS simply state that S_T for hydrocarbon flames increases linearly with u' above the baseline value of the laminar flame speed S_L at a slope of K. This slope is an empirical correlation constant derived from the experimental measurements.[1] The first term on the RHS tends to a small value at large bulk flow velocity U_0 because the laminar flame speeds of typical hydrocarbon and hydrogen flames at the ultra-lean operating conditions of gas turbines are on the order of 0.2–0.3 m/s. The second term on the RHS is a constant because turbulence in the center core of the LSI is controlled by the perforated plate and

[1]Linear dependency of S_T on u' is not universal as S_T in other burners tends to be nonlinear and shows "bending" [15].

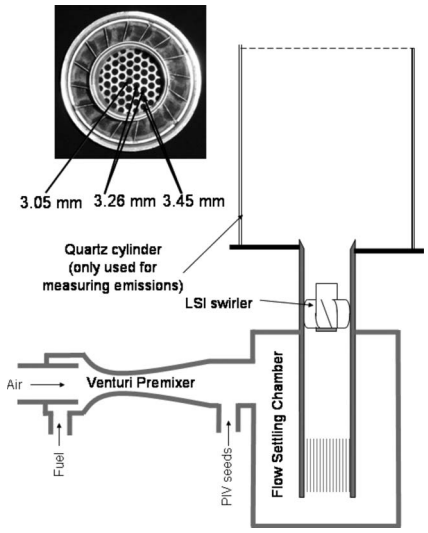

Fig. 2 Schematics of the LSI setup for atmospheric studies

scales with U_0. On the left hand side, self-similar means that $a_x=dU/dx/U_0$ in the second term is constant. The main consequence is that for a given value of K the flame position x_f-x_0 has an asymptotic value at large U_0. Therefore, when S_L is held constant at a certain ϕ, significant flame shift, i.e., changes in x_f, occurs only at low velocities where U_0 is in the same order as S_L. When $U_0 \gg S_L$, changing stoichiometry and/or U_0 do not generate significant flame shift.

Equation (2) is a simple linear analytical expression that describes the relationship between the LSI flowfield and the turbulent flame properties. Because the aerodynamic stretch rate is proportional to the swirl number [8], this expression is a convenient top order model to show how the LSI can be adjusted to accept different fuels.

3 Experimental Apparatus and Diagnostics

The LSI referred to as LSI-LH1 in our previous study [3] was chosen for our atmospheric studies on syngas operation because it can accept fuels with high H_2 concentrations. It is 6.35 cm in diameter with a center-channel of 4 cm in diameter. The swirler from Solar Turbines described earlier is recessed 9.5 cm from the exit. The center-channel plate has variable hole sizes, as shown in the insert of Fig. 2. By measuring the effective areas of the center-channel covered by the plate and the swirl annulus, the ratio of the flows through the unswirled and the swirled passages m is 0.39 to give a swirl number of $S=0.51$. The LSI was mounted vertically on top of a cylindrical settling chamber (Fig. 2). Air supplied by a fan blower entered at the side of a 25.4 cm diameter chamber and flowed into the LSI via a centrally placed 30 cm long straight feed-tube. To produce a uniform flow into the LSI, a perforated screen was placed 5 cm upstream. The air flow rate was adjusted by a computer controlled valve and monitored by a turbine meter. Fuel was injected into a commercial venturi premixer to ensure a supply of homogeneous mixture to the injector. Both the fuel and the PIV seeder flows were controlled by electronic mass flow controllers and set according to a predetermined value of mixture compositions and ϕ. The fuel and air supply system had a maximum capacity of 65 g/s to deliver maximum bulk flow velocity $U_0=22$ m/s.

Flowfield information on the open flames was obtained using PIV. The PIV system consists of a New Wave Solo PIV laser with double 120 mJ pulses at 532 nm and a Kodak/Red Lake ES 4.0 digital camera with 2048×2048 pixel resolution. The optics captured a field of view of approximately 13×13 cm^2 covering the nearfield and the farfield of the flames with 0.065 mm/pixel reso-

Table 1 Syngas compositions and conditions for the PIV experiments

Name	Composition	ϕ	T_{ad} (K)	S_L (m/s)
SG1	0.2 H_2–0.4 CO–0.4 CH_4	0.52	1591	0.14
		0.58	1708	0.18
SG2	0.3 H_2–0.3 CO=0.4 CO_2	0.55	1575	0.14
		0.64	1698	0.22
SG3	0.6 H_2–0.4 CO	0.45	1586	0.22
		0.5	1696	0.29

lution. A cyclone type particle seeder seeds the air flow with 0.6–0.8 μm Al_2O_3 particles, which should track velocity fluctuations up to 10 kHz [16].

Data acquisition and analysis were performed using a software developed by Wernet [17]. Because of the complex and 3D nature of the swirling flowfield, care had to be taken to optimize interframe timing, camera aperture setting, light sheet thickness, and seed density to ensure high data fidelity. Using a portion of the light sheet with approximately 1.1 mm thickness (away from the 0.3 mm waist produced by the 450 mm spherical lens) and a short interframe time (25 μs) helped to freeze the out-of-plane motion of seed particles. Sets of 224 image pairs were recorded for each experiment corresponding to minimum criterion required to produce stable mean and rms velocities. The PIV data were processed using 64×64 pixel cross-correlation interrogation regions with 25% overlap. This rendered a spatial resolution of approximately 2 mm. The velocity statistics were checked to ensure that significant spatial bias or "peak-locking" was not taking place.

The NO_x and CO emissions from the syngas flames were measured by enclosing the flame in a 30 cm long quartz cylinder, 20 cm in diameter (Fig. 2) to prevent the entrainment of ambient air into the combustion products. A water cooled sampling probe was placed at the center of the quartz tube at the exit. The samples were dried by a desiccant before being analyzed by a Horiba PG-250 analyzer that was calibrated using 7.9 ppm NO in nitrogen and 31.8 ppm CO in nitrogen (Scott Specialty Gases, Plumsteadville, PA). The instrument has an accuracy of ±0.5 ppm for NO_x measurements.

Tests of the LSI syngas operations at gas turbine conditions were performed in an optically accessible pressurized combustor. The facility uses a 7.6 cm diameter quartz tube to simulate the combustor casing. Therefore, it can only accommodate a reduced scale LSI. The LSI chosen for these pressurized tests is based on the design of Hwang et. al. [18]. It has a diameter of 2.54 cm with a swirler with a $R=0.55$ center-channel and eight straight blades at $\alpha=45$ deg. Hwang et. al. [18] operated this reduced scale LSI at 1–5 atm but at a relatively low bulk flow velocity of 3 m/s. To configure the LSI for velocities >25 m/s, laboratory atmospheric pressure tests were performed to select the perforated plate that will give optimum flame positions and lean blow-off. The LSI configured with this process has a swirl number of 0.425.

4 Results

4.1 Atmospheric Pressure Experiments. The compositions of the three simulated syngases chosen for the atmospheric pressure laboratory studies are listed in Table 1. They represent the syngases generated by various gasification processes. The laminar flame speeds are determined from the "premix" module of CHEMKIN using GRI 3.0.

To start, lean blow-off limits for the three syngases were determined at bulk flow velocities of 7 m/s$<U_0<$20 m/s. The results are shown in Fig. 3 together with the blow-off limits obtained previously for CH_4, diluted CH_4, and H_2. From Fig. 3, it is

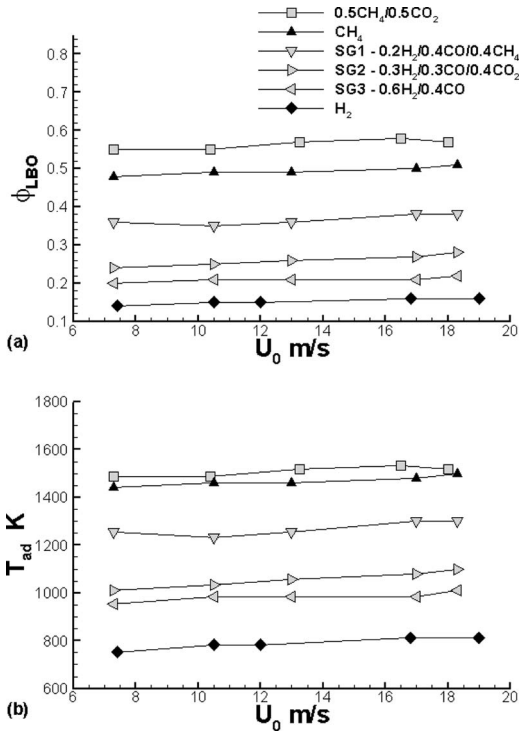

Fig. 3 Lean blow-off limits determined for simulated dry syngases CH_4 and H_2

clear that the lean blow-off limits of the syngases have the same trend as all the other fuels in that they are relatively insensitive to the bulk flow velocity U_0. The equivalence ratio ϕ and the adiabatic flame temperature T_{ad} at which blow-off occur decrease with increasing H_2 concentration and provide more evidence to show that the addition of H_2 promotes flammability. A comparison of the lean blow-offs for SG1 and SG2 illustrates the effectiveness of H_2 addition. SG1 has a higher heat content and 10% less H_2 than SG2. But SG2 blows off at T_{ad} of about 100 K lower than SG1.

The NO_x and CO emissions from the syngas flames are shown in Fig. 4. These measurements were made with the air supplied to the LSI at 27 g/s ($U_0\approx10$ m/s). In Fig. 4(*a*), the NO_x emissions from syngas flames are shown to be consistent with those from the hydrocarbon flames at STP and at gas turbine conditions [1,4,5]. This is the same conclusion from an earlier study by Sequera and Agrawal [6]. Due to the high flammability of the syngases, the flames burn at low T_{ad}, where NO_x can be <1 ppm (at 15% O_2). Though the uncertainties of the emissions data at these conditions are relatively high (±0.5 ppm) the NO_x data from syngases provide more evidence to support the log-linear dependency of LSI NO_x on T_{ad}.

The CO emissions shown in Fig. 4(*b*) are mostly below 20 ppm. The exceptions are for SG1 and a fuel with 0.5 H_2/0.5 CO at 1500 K$<T_{ad}<$1900 K. These modest increases in CO concentrations do not seem to correspond to the CO concentrations in the fuels but their trends (i.e., CO decreasing with decreasing T_{ad} and ϕ) are consistent with insufficient residence time for CO burnout to occur. In their study of LSI firing with syngases, Sequera and Agrawal [6] reported NO_x and CO concentrations at different locations downstream of the flame. They found that the CO concentrations just downstream of syngas flames with the same T_{ad} can differ by almost an order of magnitude. But with sufficient residence time for burnout to occur, their CO concentrations are compatible at the enclosure exit. Therefore, the differences shown in Fig. 4(*b*) may be attributed to the short residence

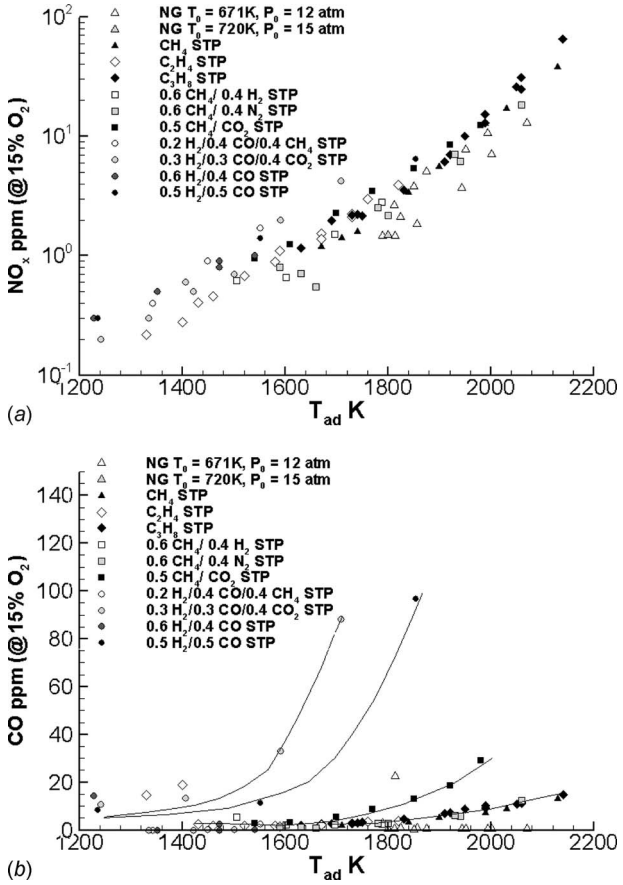

Fig. 4 NO_x and CO emissions of LSI fueled with syngases compared with results from other LSI tests with hydrocarbons and hydrogen at laboratory and gas turbine conditions

time of our experiments (about 10 ms) compared to the Sequera and Agrawal experiments (about 30 ms).

Table 1 also lists the mixtures used for the PIV experiments. The reactant compositions were set at the conditions corresponding to $T_{ad} \approx 1600$ K and 1700 K. For each mixture, PIV measurements were made at three bulk flow velocities $U_0 = 10$, 14, and 18 m/s.

Shown in Fig. 5 are the normalized mean velocity vectors for the flames at $U_0 = 14$ m/s and $T_{ad} \approx 1600$ K. It can be seen that the overall features of the flowfields are not significantly different. In the nearfield ($x/D < 0.5$), the divergent nature of the flow is shown by the outward pointing vectors. The flow discharge angles (outlined by the blue and red contours of high shear stress region of the outer mixing layers) of the three cases are also quite similar. The main differences are shown in the farfield where the SG1 and SG2 flames generated small central recirculation zones while the SG3 flame did not generate recirculation. The reason for the difference may be explained by the differences in their flame dynamics. In premixed turbulent flames, heat release through the thin reaction zone is accompanied by a sharp increase in the flow velocity [19]. This velocity jump Δu can be estimated by $\Delta u = S_L(\tau - 1)$ where τ is the expansion ratio T_{ad}/T_0. For the three flames in Fig. 5, their τ values are the same but their S_L are not. From Table 1, it can be seen that Δu in the SG3 flame is about 50% higher. The consequence of the larger velocity jumps across the flame fronts is evident by comparing the lengths of the velocity vectors at $x/D > 0.5$. Due to the higher axial momentum generated in the product region of SG3, the central recirculation is not formed as all the velocity vectors leaving the upper boundary of the PIV domain are positive. These results demonstrate that the farfield features of the LSI are coupled to the flame/turbulence interactions at the flame fronts. The presence and the absence of the central recirculation zone are artifacts of the dynamic processes associated with the interactions.

The centerline profiles of the syngas flames with $T_{ad} \approx 1600$ K are shown in Fig. 6. Because these flame brushes are close to the LSI exit, only a very small portion of their nearfield linear velocity decay regions is shown (Fig. 6(*a*)). As a consequence, the parameters to characterize the nearfield region, i.e., the virtual origin x_0 of the divergent flow and normalized axial divergence rate $a_x = \delta U/\delta x/U_0$ [4], cannot be determined from these data with a high degree of confidence. Therefore, these axial profiles can only be used to compare the velocity distribution downstream of the flame brush where the flow accelerations associated with the higher Δu from the SG3 flames can be seen. Profiles of the normalized 2D turbulent kinetic energy $q' = ((u'^2 + v'^2)^{1/2})/2$ of Fig. 6(*b*) show that turbulence along the centerline remains relatively constant. This is the same behavior observed in most of the other hydrocarbon flames.

Radial profiles for the syngas flames with $T_{ad} \approx 1600$ K are shown in Fig. 7. These profiles were extracted at $x = 10$ mm just below the flame brushes. Unlike the axial profiles, the radial pro-

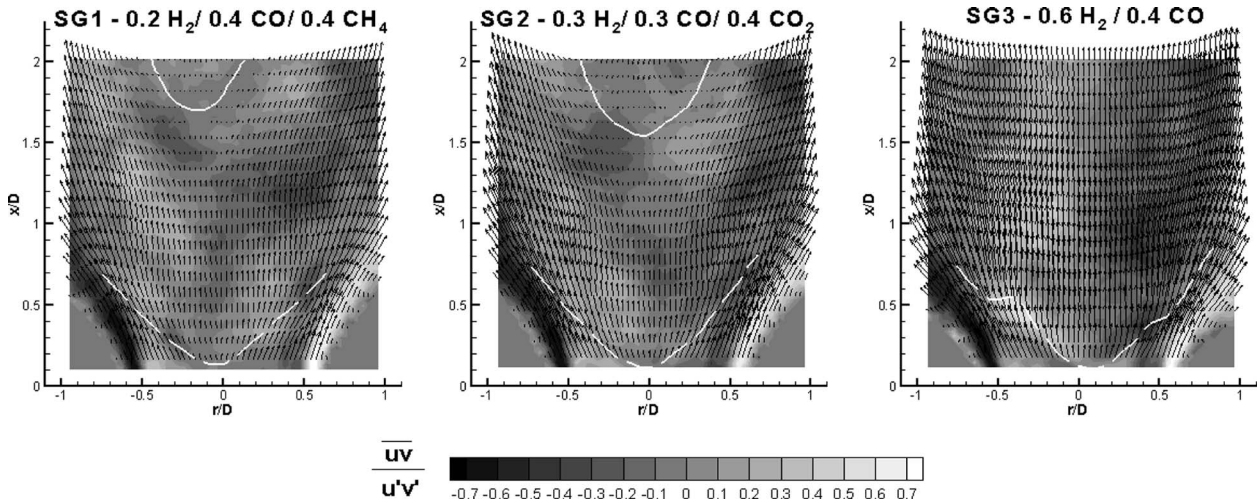

Fig. 5 Normalized velocity vectors for syngas flames at $U_0 = 14$ m/s and $T_{ad} \approx 1700$ K. The top continuous lines mark the boundaries of the recirculation bubble, and lower dashed lines mark the leading edges of the flame brushes.

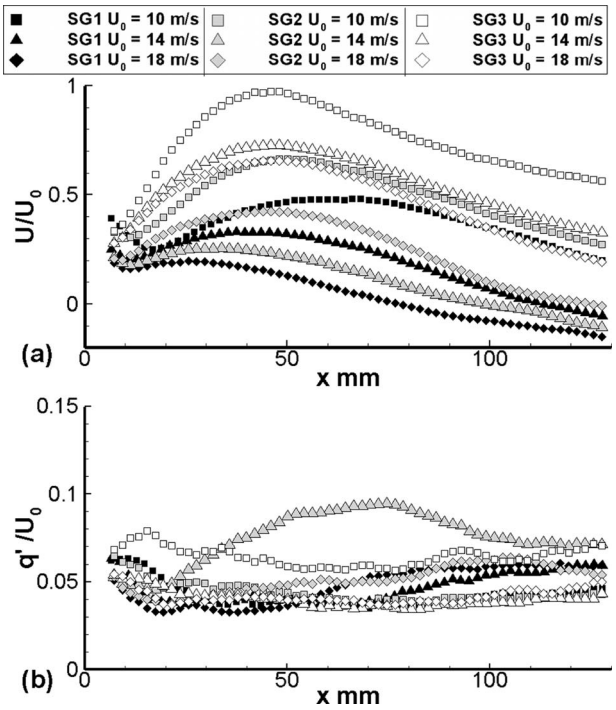

Fig. 6 Centerline profiles of the syngas flames with $T_{ad} \approx 1600$ K: (*a*) mean axial velocity and (*b*) turbulent kinetic energy

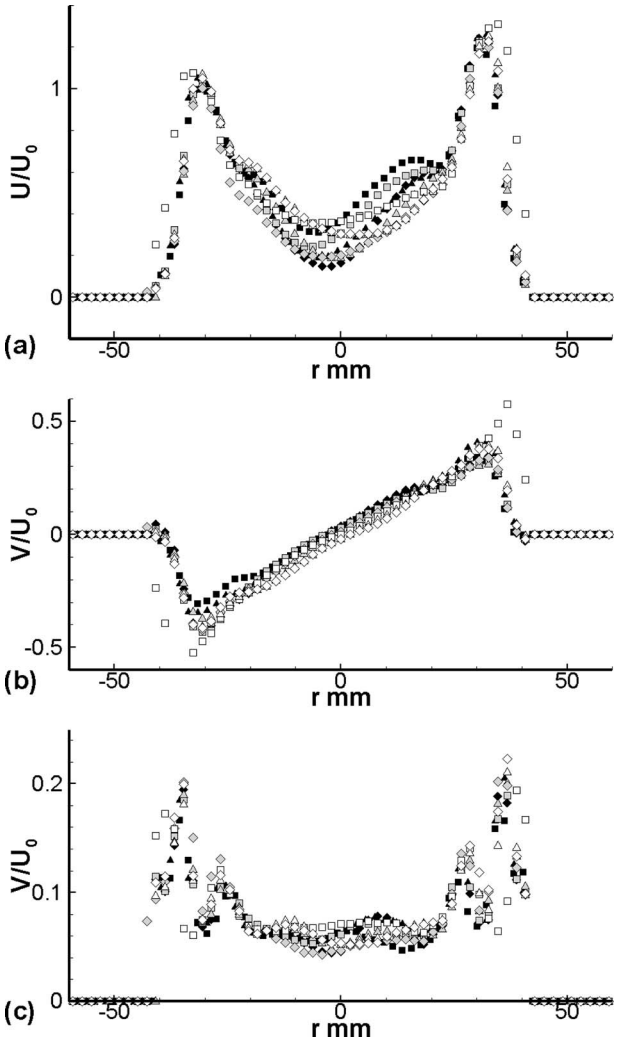

Fig. 7 Radial profiles (at $x=10$ mm) of the syngas flames with $T_{ad} \approx 1600$ K: (*a*) mean axial velocity, (*b*) mean radial velocity, and (*c*) turbulent kinetic energy. Legend same as for Fig. 6.

files collapse onto consistent trends to show self-similar behavior. In Fig. 7(*a*), the U/U_0 profiles have a central low velocity region that has a deficit corresponding to the nonswirling flow supplied through the center-channel. The central nonuniform distribution is a feature of this LSI that uses a perforated plate with varying hole size [3]. Variation in U/U_0 within the core regions corresponds to the scatter in U/U_0, as shown in Fig. 6(*a*), at $x=10$ mm. The two velocity peaks flanking the central region correspond to the swirling flow. In Fig. 7(*b*), the linear regions of the V/U_0 profiles within the center region (-15 mm $< r <$ 15 mm) show that the normalized radial divergence rates $a_r = \delta V/\delta r/U_0$ are nearly the same for all cases and averaged about 0.012 mm^{-1}. In the absence of the normalized axial divergence rate data, the a_r data provide the evidence to show that the nearfields of the syngas flames are self-similar. However, the values of a_r are higher than those found in the hydrocarbon flames and seem to be a consequence of the close proximity of the flame brush to the LSI exit. The q'/U_0 profiles (Fig. 7(*c*)) have relatively flat distributions in the center regions surrounded by intense turbulence peaks. These features are the same as those found in all other LSI flames.

The local turbulent flame speed S_T at the LSI centerline is the basic turbulent flame property that explains the LSI stabilization mechanism because the freely propagating flame settles at the point within the center divergent flow region where the mean flow velocity is equal and opposite to S_T. From previous studies using low-swirl burners fitted with air jets [9,13], it has been shown that S_T/S_L correlates linearly with u'/S_L. More recent data from the CH_4/air LSI flames at 7 m/s $< U_0 <$ 22 m/s [4] and from two 5.08 cm ID LSBs of $R=0.8$ and 0.6 [8] give further support to this correlation.

The S_T for the syngas flames were also deduced from the current data set but because of the close proximity of the SG3 flames to the LSI exit, only three out of the six flames were deemed suitable for extracting reliable S_T information. Figure 8 compares the S_T obtained for the 15 syngas flames together with all previous S_T measurements from the LSI. This plot differs from previous S_T plots in two significant respects. First of all, it contains S_T data obtained only in the LSI whereas previous plots include data from all other low-swirl burners. Second, recent S_L values for unstretched laminar flames were used for the normalization [20]. The most significant change is the new S_L values at the ultralean conditions being much higher than the old. Due to this difference, the maximum values of S_T/S_L and u'/S_L for our data set are reduced. However, the adjustment does not change the linear increasing trend of S_T/S_L with u'/S_L or the correlation constant K. The value of K for the methane/air flames generated by the LSI is 1.73. This is slightly lower than the value of 2.14 obtained by including the S_T data from all the other low-swirl burners. The correlation constant K of 3.15 for the H_2 flames is the same because only the LSI has been used for H_2 flame studies.

Figure 8 shows that the S_T of syngas flames are between those for methane and hydrogen and the results for each syngas exhibit linear dependencies on u' but with slight differences in their turbulent flame speed correlation constants. These trends show that the syngas turbulent flame speed behaves in ways that are consistent with previous conclusion. That is, the primary effect of H_2 addition is to increase the S_T correlation constant K. Based on the analytical model Eq. (2), an increase in K implies a slight decrease in the flame brush position if the swirl number and the bulk flow velocity of the LSI are held constant. This is verified qualitatively

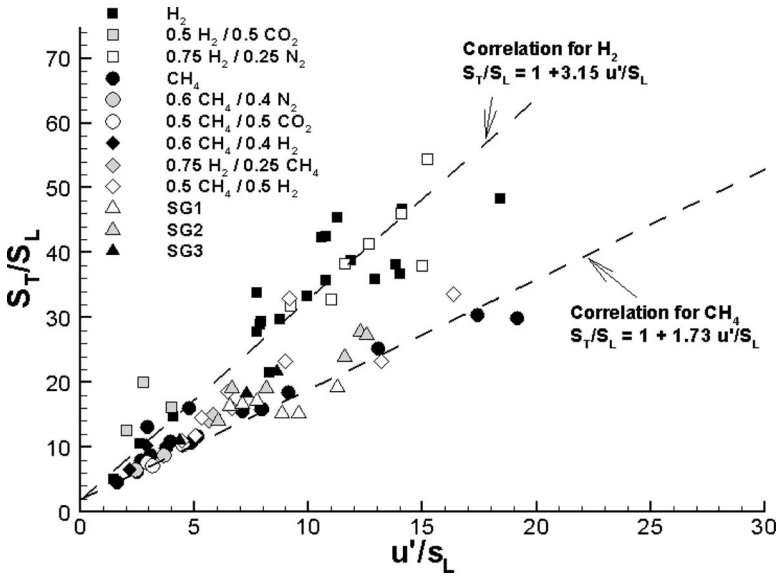

Fig. 8 Turbulent flame speed correlation for LSI flames with fuel blends consisting of H_2, CH_4, CO, N_2, and CO_2

by the lowered flame brush positions of the high H_2 content SG3 flames as mentioned above.

4.2 High Pressure Experiments. A series of tests was performed with CH_4 and H_2/CH_4 blends to verify the compatibility of the reduced-scale LSI with the pressurized combustor and to obtain baseline lean blow-off limits. The experimental conditions covered a nozzle exit velocity range of 20–40 m/s, temperatures at 450 K $< T <$ 505 K, and pressures at 1.5 atm $< P <$ 14 atm. The flame was monitored by a standard JVC camcorder at 30 fps and thermocouples mounted at various positions on the combustor and in the LSI. Although the lean blow-off limits of the reduced-scale LSI are consistent with those observed in other systems, the experience indicated that this LSI with straight swirler blades is not highly compatible with the pressurized combustor because the optimum operating range is restricted to $U_0 < 20$ m/s. Therefore, the high pressure syngas experiments were mostly conducted at the low velocity range.

The compositions of the fuels tested at 450 K $< T <$ 505 K and $P = 8$ atm are shown as circular dots in Fig. 9 where the corners of the triangle represent 100% concentration. The ranges of the concentrations for each component are $20\% < H_2 < 56\%$, $25\% <$ CO $< 60\%$, and $19\% < CH_4 < 51\%$. The equivalence ratios tested, shown in Fig. 10, varied from 0.3 to 0.55 corresponding to adiabatic flame temperatures of 1350 K $< T_{ad} <$ 1800 K. These experiments were performed by starting with a CH_4 flame and adding H_2 and CO into the fuel stream while the flame was lit.

Four representative images are shown in Fig. 11 to illustrate the flame shape as determined from a single video frame. Figure 11(*a*) shows a flame with low H_2 fuel concentration and it assumes a bowl shape similar to the open flame of Fig. 1. The flame is lifted from the LSI though it is not obvious from the camcorder image because the LSI exit is obscured by the lip of the mounting flange of the quartz liner. Figure 11(*b*) shows one of the few syngas flames studied at higher velocity of 31 m/s. The shape and location of this lean $\phi = 0.28$ flame are not very different than the flame of Fig. 11(*a*). The flame in Fig. 11(*c*) is not very discernable due to the apparent increase in background luminosity by the camcorder's built-in auto-exposure feature that compensated for the reduction in luminosity of this flame burning a syngas with a higher 15% H_2 concentration. However, the region of high luminosity associated with the flame impingement on the quartz liner suggests that the position of the flame is relatively unaffected by the change in fuel composition. Figure 11(*d*) shows the image of a syngas flame with 51% H_2 that has very low luminosity. The useful information provided by this image is that significant flame shift does not seem to occur with the higher H_2 fuel concentration.

These syngas flame images show that the flame position and to a lesser extent the flame shape are not significantly changed at high temperatures and pressures. Although the test conditions were limited, the range of the fuel compositions explored and the

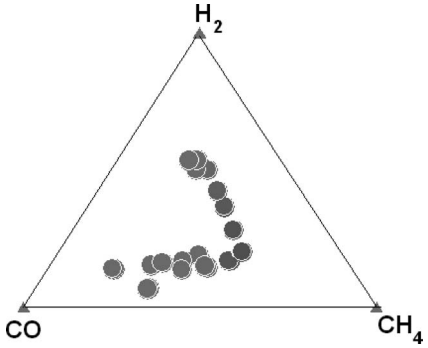

Fig. 9 Syngas compositions evaluated at a 75 cm ID pressurized combustor

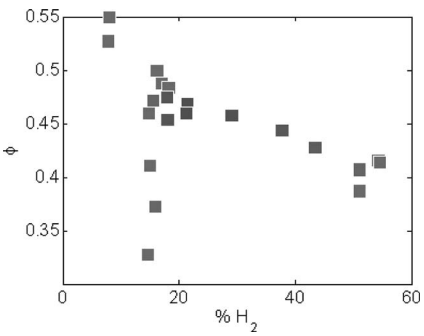

Fig. 10 Equivalence ratios of the high pressured syngas experiments

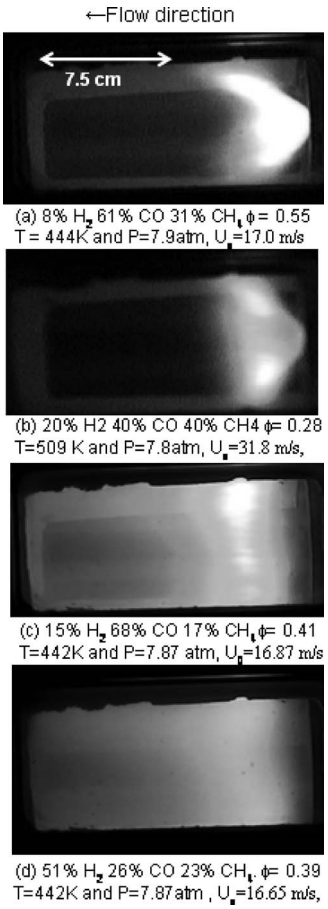

Fig. 11 Luminosity images of syngas flames generated by a reduced scale LSI captured by a camcorder

fact that the LSI can easily transition from one fuel composition to the next demonstrated the viability of this concept for syngases.

5 Conclusion

Open laboratory flames generated by a full size LSI (6.35 cm) were used to investigate the lean blow-off limits, emissions, and the flowfield characteristics. The results show that the basic LSI design is amenable to burning syngases with H_2 up to 60%. Syngases with high H_2 concentration have lower lean blow-off limits to show the effectiveness of H_2 addition to enhance flammability. The PIV measurements show that the overall features of the flowfields of the syngas flames are the same as those found in the hydrocarbon and the hydrogen flames. The nearfields show similarity behavior and the turbulent flame speeds correlate linearly with turbulence intensity u'. These results show that the analytical model developed for the LSI is also valid for syngases. The main implication is that the syngas flame positions change with the H_2 concentration due to the increase in the turbulent flame speed correlation constant K. The NO_x emissions from syngas flames show log-linear dependency on the adiabatic flame temperature and are comparable to those reported for the gaseous fuels reported previously. Verification of syngas operation at elevated temperatures and pressures were performed with a reduced scale (2.54 cm) LSI in a small pressurized combustion channel. Successful firing of the reduced-scale LSI at 450 K $<$ T $<$ 505 K and 8 atm verified the operability of this concept at gas turbine conditions.

Acknowledgment

This work was supported by the U.S. Department of Energy, Office of Fossil Energy under Contract No. DE-AC02-05CH11231.

Nomenclature

$a_x = dU/dx/U_0$ = normalized axial flow divergence (1/mm)
$a_r = dV/dr/U_0$ = normalized radial flow divergence (1/mm)
L_i = swirler recess distance
$m = m_c/m_s$ = mass flux ratio
m_c = mass flux through center channel
m_s = mass flux through swirl annulus
q' = 2D turbulent kinetic energy $= \frac{1}{2}(u'^2 + v'^2)^{1/2}$
Re = Reynolds number $2R_iU_0/\nu$
$R = R_c/R_i$ = ratio of the center channel radius R_c to injector radius R_i
R = radial distance
S = swirl number
S_L = laminar flame speed
S_T = turbulent flame speed
T_{ad} = adiabatic flame temperature
U_0 = bulk flow velocity
U = axial velocity
u' = axial rms velocity
v' = radial rms velocity
uv = shear stress
x = axial distance from injector exit
x_f = leading edge position of the flame brush
x_o = virtual origin of divergent flow

References

[1] Johnson, M. R., Littlejohn, D., Nazeer, W. A., Smith, K. O., and Cheng, R. K., 2005, "A Comparison of the Flowfields and Emissions of High-Swirl Injectors and Low-Swirl Injectors for Lean Premixed Gas Turbines," Proc. Combust. Inst., **30**, pp. 2867–2874.
[2] Nazeer, W. A., Smith, K. O., Sheppard, P., Cheng, R. K., and Littlejohn, D., 2006, "Full Scale Testing of a Low Swirl Fuel Injector Concept for Ultra-Low NO_x Gas Turbine Combustion Systems," ASME Paper No. GT2006-90150.
[3] Cheng, R. K., and Littlejohn, D., 2008, "Laboratory Study of Premixed H2-Air & H_2–N_2-Air Flames in a Low-Swirl Injector for Ultra-Low Emissions Gas Turbines," ASME J. Eng. Gas Turbines Power, **130**(5), pp. 31503-1–31503-9.
[4] Cheng, R. K., Littlejohn, D., Nazeer, W. A., and Smith, K. O., 2008, "Laboratory Studies of the Flow Field Characteristics of Low-Swirl Injectors for Application to Fuel-Flexible Turbines," ASME J. Eng. Gas Turbines Power, **130**(2), p. 021501.
[5] Littlejohn, D., and Cheng, R. K., 2007, "Fuel Effects on a Low-Swirl Injector for Lean Premixed Gas Turbines," Proc. Combust. Inst., **31**(2), pp. 3155–3162.
[6] Sequera, D., and Agrawal, A. K., 2007, "Effects of Fuel Composition on Emissions From a Low-Swirl Burner," ASME Paper No. GT2007-28044.
[7] Chan, C. K., Lau, K. S., Chin, W. K., and Cheng, R. K., 1992, "Freely Propagating Open Premixed Turbulent Flames Stabilized by Swirl," Sym. (Int.) Combust., [Proc.], **24**, pp. 511–518.
[8] Cheng, R. K., Yegian, D. T., Miyasato, M. M., Samuelsen, G. S., Pellizzari, R., Loftus, P., and Benson, C., 2000, "Scaling and Development of Low-Swirl Burners for Low-Emission Furnaces and Boilers," Proc. Combust. Inst., **28**, pp. 1305–1313.
[9] Bedat, B., and Cheng, R. K., 1995, "Experimental Study of Premixed Flames in Intense Isotropic Turbulence," Combust. Flame, **100**(3), pp. 485–494.
[10] Cheng, R. K., 1995, "Velocity and Scalar Characteristics of Premixed Turbulent Flames Stabilized by Weak Swirl," Combust. Flame, **101**(1–2), pp. 1–14.
[11] Plessing, T., Kortschik, C., Mansour, M. S., Peters, N., and Cheng, R. K., 2000, "Measurement of the Turbulent Burning Velocity and the Structure of Premixed Flames on a Low Swirl Burner," Proc. Combust. Inst., **28**, pp. 359–366.
[12] Shepherd, I. G., and Cheng, R. K., 2001, "The Burning Rate of Premixed Flames in Moderate and Intense Turbulence," Combust. Flame, **127**(3), pp. 2066–2075.
[13] Cheng, R. K., Shepherd, I. G., Bedat, B., and Talbot, L., 2002, "Premixed Turbulent Flame Structures in Moderate and Intense Isotropic Turbulence," Combust. Sci. Technol., **174**(1), pp. 29–59.
[14] Bell, J. B., Day, M. S., Shepherd, I. G., Johnson, M. R., Cheng, R. K., Grcar,

J. F., Beckner, V. E., and Lijewski, M. J., 2005, "Numerical Simulation of a Laboratory-Scale Turbulent V-Flame," Proc. Natl. Acad. Sci. U.S.A., **102**(29), pp. 10006–10011.
[15] Lipatnikov, A. N., and Chomiak, J., 2002, "Turbulent Flame Speed and Thickness: Phenomenology, Evaluation, and Application in Multi-Dimensional Simulations," Prog. Energy Combust. Sci., **28**(1), pp. 1–74.
[16] Melling, A., 1997, "Tracer Particles and Seeding for Particle Image Velocimetry," Meas. Sci. Technol., **8**, pp. 1406–1416.
[17] Wernet, M. P., 1999, "Fuzzy Logic Enhanced Digital PIV Processing Software," 18th International Congress on Instrumentation for Aerospace Simulation Facilities, Toulouse, France.
[18] Hwang, Y., Ratner, A., and Bethel, B., 2007, "Chamber Pressure Perturbation Coupling With a Swirl-Stabilized Lean Premixed Flame at Elevated Pressures," Fifth U.S. Combustion Meeting, Western States Section of the Combustion Institute, San Diego.
[19] Cheng, R. K., 1984, "Conditional Sampling of Turbulence Intensities and Reynolds Stress in Premixed Flames," Combust. Sci. Technol., **41**, pp. 109–142.
[20] Jomaas, G., Zheng, X. L., Zhu, D. L., and Law, C. K., 2005, "Experimental Determination of Counterflow Ignition Temperatures and Laminar Flame Speeds of C_2–C_3 Hydrocarbons at Atmospheric and Elevated Pressures," Proc. Combust. Inst., **30**(1), pp. 193–200.